MITIGATING SPURIOUS CORRELATIONS VIA GROUP-ROBUST SAMPLE REWEIGHTING

Anonymous authors
Paper under double-blind review

ABSTRACT

Machine learning models often have uneven performance among subpopulations (a.k.a., groups) in the data distributions. This poses a significant challenge for the models to generalize when the proportions of the groups shift during deployment. To improve robustness to such subpopulation shifts, existing approaches have developed strategies that train models or perform hyperparameter tuning using the group-labeled data to minimize the worst-case loss over groups. However, a non-trivial amount of high-quality labels is often required to obtain noticeable improvements. Given the costliness of the labels, we propose to adopt a different paradigm to enhance group label efficiency: utilizing the group-labeled data as a target set to optimize the weights of other group-unlabeled data. We introduce a two-stage approach called Group-robust Sample Reweighting (GSR) that first learns the representations from group-unlabeled data, and then tinkers the model by iteratively retraining its last layer on the reweighted data. Our GSR is theoretically sound, practically lightweight, and effective in improving the robustness to subpopulation shifts. In particular, GSR outperforms the previous state-of-the-art results on standard benchmarks when using the same amount of group labels. Notably, GSR even outperforms approaches that require significantly more group labels.

1 INTRODUCTION

Subpopulation shift refers to the change in the proportion of groups (as defined by the class, attributes, or both) in data distribution between the training and deployment phases (Koh et al., 2021; Yang et al., 2023). Due to the nature of subpopulations or the selection bias (Dwork et al., 2012; Zadrozny, 2004), the training data is often composed of majority and minority groups that are overrepresented and underrepresented, respectively. Common examples include photos of waterbirds frequently being taken with a water background instead of the land background and pairs of sentences with contradictions often being accompanied by negation words (Sagawa et al., 2019). Such group imbalance can cause some features from the majority group to be spuriously correlated with the labels, leading to possible undesirable shortcuts in training deep neural networks (Geirhos et al., 2020; Hermann et al., 2024; Shah et al., 2020). As a result, standard training with empirical risk minimization (ERM) often overly relies on such shortcuts and fails to attend to the minority groups, leading to worsened model generalization under subpopulation shifts, especially when the proportion of the minority groups increases (Arjovsky et al., 2019; Nagarajan et al., 2020; Sagawa et al., 2020). Thus, it is important to develop algorithms that are group-robust to subpopulation shifts, experiencing minimal performance degradation as measured by the worst-group accuracy.

The group labels can be used to construct balanced groups or minimize the worst-group loss during training (Idrissi et al., 2022; Sagawa et al., 2019). These techniques often lead to improved group robustness compared to ERM. However, group labels can be expensive to obtain, necessitating approaches that maximize the gain in group robustness from limited data. Given a group-labeled dataset $\mathcal{D}^{\mathrm{L}}$, the two mainstream categories are either using $\mathcal{D}^{\mathrm{L}}$ for model selection (Liu et al., 2021; Zhang et al., 2022), or using $\mathcal{D}^{\mathrm{L}}$ to directly train the model parameters (Kirichenko et al., 2022). However, these strategies may not always be the best way to exploit the group information, since they either underutilize the group labels, or restrict the most crucial part of the training to only $\mathcal{D}^{\mathrm{L}}$ while neglecting the potential of the more accessible data without group labels. Therefore, we advocate an in-between training paradigm: instead of using $\mathcal{D}^{\mathrm{L}}$ to train the model parameters directly, we use

them to iteratively optimize the weights of a group-unlabeled dataset $\mathcal{D}^{\text{U}}$, which are more realistic to obtain. Then, the model parameters are trained using a weighted objective on these data with ERM.

Optimizing the sample weights is an established idea that necessitates solving a bilevel optimization problem (Ren et al., 2018). The inner loop of the bilevel optimization performs standard model training on a weighted objective, while the outer loop optimizes the sample weights. The two main challenges hindering its wider adoption include: (1) the unavoidable trade-off between computational cost and accuracy, and (2) the effectiveness when the model is overparameterized. For (1), calculating the outer loop gradient requires backpropagating through the entire training process, which is computationally prohibitive for deep neural networks. Conventional approaches use a one-step truncated backpropagation that relies only on the last-step gradient of the model training for computational feasibility (Shaban et al., 2019; Zhou et al., 2022). However, this approximation can be imprecise as it fails to account for the curvature of the loss landscape and the training dynamics of the model. For (2), training a weighted objective with overparameterized neural networks is likely to converge to the same solution as with ERM (Sagawa et al., 2019; Zhai et al., 2022). Regularization techniques need to be applied such that training with weighted objectives leads to meaningfully different solutions than using ERM (Byrd & Lipton, 2019; Sagawa et al., 2019; Zhai et al., 2022).

To address the two challenges, we propose a simple two-stage method named Group-robust Sample Reweighting (GSR), which iteratively reweights individual training samples to improve group robustness. We utilize last-layer retraining (LLR), a lightweight method that retrains the last linear layer of neural network (Kang et al., 2020; Kirichenko et al., 2022). LLR simplifies the inner loop of the bilevel optimization into a convex optimization problem. Importantly, it facilitates our application of the influence function, a technique derived from implicit differentiation (Koh & Liang, 2017; Krantz & Parks, 2002), to utilize the Hessian to accurately estimate the gradient of sample weight updates without backpropagating through the entire training trajectory. In contrast to methods that rely on one-step truncated backpropagation approximations (Zhou et al., 2022), our approach leverages the fact that LLR is both inexpensive even with Hessian computation and effective for enhancing group robustness. To perform GSR, we split the group-unlabeled dataset $\mathcal{D}^{\text{U}}$ into a held-out set $\mathcal{D}^{\text{U-h}}$ and a remaining set $\mathcal{D}^{\text{U-r}}$. The first stage performs unweighted representation learning on $\mathcal{D}^{\text{U-r}}$. The second stage utilizes the influence function to iteratively optimize the weights of $\mathcal{D}^{\text{U-h}}$ for the worst-group loss in $\mathcal{D}^{\text{L}}$ achieved through LLR. Our method achieves an average improvement of 1.0% in terms of absolute worst-group accuracy as compared to the state-of-the-art method that uses the same amount of group labels as ours and outperforms methods that require more group labels.

The specific contributions of this work include the following:

- We propose to better leverage the high-quality group-labeled data for group robustness with an alternative paradigm by using them to reweight other samples instead of directly training on them.
- We devise an efficient strategy based on implicit differentiation for group-robust sample reweighting, which becomes accurate and computationally feasible via the synergy with last-layer retraining.
- We empirically demonstrate the performance advantages of our lightweight approach on improving the group robustness for both vision and natural language tasks.

2 Problem Formulation and Preliminaries

Let $(\mathcal{X}, \mathcal{Y}, \mathcal{G})$ denote the space of input, class label, and groups of subpopulation respectively. Denote a dataset by $\mathcal{D} = \{z_1, \ldots, z_n\}$, where each data point $z_i := (x_i, y_i, g_i) \in \mathcal{X} \times \mathcal{Y} \times \mathcal{G}$ is sampled i.i.d. from a data distribution $\mathcal{P}$. For $g \in \mathcal{G}$, define $\mathcal{D}_g := \{z_i \in \mathcal{D} | g_i = g\}$ as the subset of data from group g, sampled from the group data distribution $\mathcal{Q}_g$. We assume that $\mathcal{P}$ can be decomposed into $\mathcal{P} = \sum_{g\in\mathcal{G}} \pi_g \mathcal{Q}_g$ where the mixing ratio $\pi_g \in [0, 1]$, $\sum_{g\in\mathcal{G}} \pi_g = 1$. As a result, any subpopulation shifts can be represented by adjusting π_g. Depending on the group-label availability, datasets can be categorized as $\mathcal{D}^{\text{L}}$, $\mathcal{D}^{\text{U}}$ for group-labeled, group-unlabeled datasets. Meanwhile, depending on the functionality, datasets can be categorized as $\mathcal{D}^{\text{tr}}$, $\mathcal{D}^{\text{v}}$, $\mathcal{D}^{\text{tar}}$, denoting the training, validation, target sets, respectively. The target set $\mathcal{D}^{\text{tar}}$ guides the sample weight updates and we reserve the notion of validation set $\mathcal{D}^{\text{v}}$ only for hyperparameter and model selection. Let $N = \{1, \ldots, n\}$ be the indices of the training set. We use d for the total derivative and use ∂ or ∇ for the partial derivative.

The classic algorithms such as empirical risk minimization (ERM) focus on optimizing the model parameters θ without adjusting the data, following $\hat{\mathcal{R}}(\mathcal{D}^{\text{tr}}; \theta) = \sum_{i\in N} \frac{1}{n} \ell(x_i, y_i; \theta)$ where ℓ is the

loss function. Let $w \in \mathbb{R}^n$ be the weight vector for all training samples. A weighted training objective assigns different importance to the training data points, $\hat{\mathcal{R}}(\mathcal{D}^{\text{tr}}; w, \theta) = \sum_{i \in N} w_i \ell(x_i, y_i; \theta)$. Since the change of π is not assumed to be known at test time, we evaluate the robustness to distribution shifts of a model with parameters θ using the worst-group risk (Sagawa et al., 2019):

$$\hat{\mathcal{R}}^{\text{WG}}(\mathcal{D}; \theta) = \max_{g \in \mathcal{G}} \hat{\mathcal{R}}(\mathcal{D}_g; \theta) \ .$$

To minimize the worst-group risk, existing approaches (Kirichenko et al., 2022; Sagawa et al., 2019) have focused on directly training on group-annotated dataset $\mathcal{D}^{\text{L}}$ using the objective $\hat{\mathcal{R}}^{\text{WG}}(\mathcal{D}^{\text{L}}; \theta)$. However, these strategies require having a sufficient amount of data for each group. Alternatively, we can assume the availability of some group-unlabeled data $\mathcal{D}^{\text{U}}$ (e.g., standard training set). By viewing the sample weight vector of $\mathcal{D}^{\text{U}}$ as another set of parameters and optimizing it jointly with the model parameters w.r.t. the target set $\mathcal{D}^{\text{tar}} = \mathcal{D}^{\text{L}}$, we arrive at a bilevel formulation of the minimax problem (Zhou et al., 2022):

$$\begin{aligned} &\min_{w \in S} \max_{g \in \mathcal{G}} \hat{\mathcal{R}}(\mathcal{D}_g^{\text{tar}}; \hat{\theta}^*) \\ &\text{s.t. } \hat{\theta}^* = \arg\min_{\theta} \hat{\mathcal{R}}(\mathcal{D}^{\text{tr}}; w, \theta) \ , \end{aligned} \tag{1}$$

where $S = \{w = [w_1, w_2, \cdots, w_n] \in \mathbb{R}^n | w_i \geq 0 \, \forall i \in N, \text{ and } \sum_{i \in N} w_i = 1\}$. The inner loop performs standard model training on the weighted objective, which is typically optimized by variants of gradient descent. To optimize the sample weights of the training set in the outer loop, we can similarly perform gradient descent using its total derivative:

$$\frac{\mathrm{d}\hat{\mathcal{R}}(\mathcal{D}^{\text{tar}}; \hat{\theta}^*)}{\mathrm{d}w} = \nabla_\theta \hat{\mathcal{R}}(\mathcal{D}^{\text{tar}}; \hat{\theta}^*) \frac{\mathrm{d}\hat{\theta}^*}{\mathrm{d}w} \ .$$

Since $\hat{\theta}^*$ is typically obtained via gradient descent, calculating $\frac{\mathrm{d}\hat{\theta}^*}{\mathrm{d}w}$ (i.e., the gradient of the final model parameter $\hat{\theta}^*$ w.r.t. the sample weights w) involves unrolling the entire training trajectory and backpropagating through it, which is overly expensive to compute especially when the model is an overparameterized deep neural networks. To efficiently approximate $\frac{\mathrm{d}\hat{\theta}^*}{\mathrm{d}w}$, MAPLE (Zhou et al., 2022) adopts one-step truncated backpropagation (Shaban et al., 2019) when calculating the gradient for the outer loop:

$$\frac{\mathrm{d}\hat{\theta}^*}{\mathrm{d}w} \overset{\text{one-step}}{\approx} \nabla_w \theta_T = -\eta \frac{\partial^2 \hat{\mathcal{R}}(\mathcal{D}^{\text{tr}}; w, \theta_{T-1})}{\partial \theta \partial w} \ , \tag{2}$$

where η is the learning rate. Subsequently, w is updated with projected gradient descent. This approximation essentially relies on the last-step gradient w.r.t. each training instance z_i, i.e., $\nabla_{w_i} \theta_T = -\eta \nabla_\theta \hat{\mathcal{R}}(z_i; \theta_{T-1}) \approx -\eta \nabla_\theta \hat{\mathcal{R}}(z_i; \theta_T)$, derived in Appendix A.2. After dropping η, we can rewrite:

$$\frac{\mathrm{d}\hat{\mathcal{R}}(\mathcal{D}^{\text{tar}}; \hat{\theta}^*)}{\mathrm{d}w_i} \overset{\text{MAPLE}}{\approx} -\nabla_\theta \hat{\mathcal{R}}(\mathcal{D}^{\text{tar}}; \theta_T)^\top \nabla_\theta \hat{\mathcal{R}}(z_i; \theta_T) \ . \tag{3}$$

To interpret, MAPLE essentially updates sample weights according to the inner product between the gradient of the target loss and the gradient of the unweighted loss for each sample upon convergence. Performing bilevel optimization with this approximation is reasonable because it tends to upweight training points that share similar gradient directions with the target sets. However, this approximation is imprecise as it neither accounts for the curvature of the loss landscape w.r.t. the current model nor fully captures the training dynamics, where w_i could significantly affect the batch gradient and optimization trajectory. Prior works have discussed that deep neural networks exhibit different learning behaviors for the same data point at different steps along the training trajectory (Pleiss et al., 2020; Swayamdipta et al., 2020). Therefore, reweighting data points based solely on last-step gradients is shortsighted and can lead to suboptimal convergence.

3 GROUP-ROBUST SAMPLE REWEIGHTING VIA IMPLICIT DIFFERENTIATION

Our goal is to develop a technique that updates the sample weights for optimizing the bilevel minimax objective in Equation 1 more accurately and efficiently. In this section, we first establish the connection between reweighting samples via implicit differentiation and the influence function (Koh & Liang, 2017) from the perspective of bilevel optimization. Then, we present an effective integration

of the influence function and adaptive aggregation (Sagawa et al., 2019) to optimize the minimax objective in the outer loop.

Implicit differentiation can be used to calculate the gradient w.r.t. the sample weights without backpropagating through the inner loop of the objective according to the implicit function theorem (IFT) (Krantz & Parks, 2002). Assuming an unconstrained and strongly convex inner objective, then it implies that (1) the gradient w.r.t. the model parameters θ diminishes to zero upon convergence to the inner loop optimum, i.e., $\nabla_\theta \hat{\mathcal{R}}(\mathcal{D}^{\text{tr}}; w, \hat{\theta}^*) = 0$, and (2) the Hessian of the weighted training objective evaluated at $\theta = \hat{\theta}^*$, $H_{\hat{\theta}^*,w} \coloneqq \nabla^2_\theta \hat{\mathcal{R}}(\mathcal{D}^{\text{tr}}; w, \hat{\theta}^*)$, is invertible (Boyd & Vandenberghe, 2004). This satisfies two of the conditions required to apply the IFT. In addition, IFT further requires the inner objective to be twice continuously differentiable. We formally state the assumptions below.

Assumption 3.1. The inner objective $\hat{\mathcal{R}}(\mathcal{D}^{\text{tr}}; w, \theta)$ is unconstrained, strongly convex, and twice continuously differentiable with respect to θ, $\forall w \in S$ (Equation 1).

Although appearing as restrictive, these assumptions can be easily satisfied through last-layer retraining, as detailed in Section 4. Under Assumption 3.1, as $\nabla_\theta \hat{\mathcal{R}}(\mathcal{D}^{\text{tr}}; w, \hat{\theta}^*) = 0$, the outer gradient $\frac{\mathrm{d}\hat{\theta}^*}{\mathrm{d}w} = \left[\frac{\mathrm{d}\hat{\theta}^*}{\mathrm{d}w_1} \; \frac{\mathrm{d}\hat{\theta}^*}{\mathrm{d}w_2} \; \cdots \; \frac{\mathrm{d}\hat{\theta}^*}{\mathrm{d}w_n}\right]^\top \in \mathbb{R}^{n \times 1}$ can be calculated *exactly* via implicit differentiation as:

$$\frac{\mathrm{d}\hat{\theta}^*}{\mathrm{d}w} = -H^{-1}_{\hat{\theta}^*,w} \nabla_w \nabla_\theta \hat{\mathcal{R}}(\mathcal{D}^{\text{tr}}; w, \hat{\theta}^*) \,, \tag{4}$$

$$\frac{\mathrm{d}\hat{\theta}^*}{\mathrm{d}w_i} = -H^{-1}_{\hat{\theta}^*,w} \nabla_\theta \hat{\mathcal{R}}(z_i; \hat{\theta}^*) = -H^{-1}_{\hat{\theta}^*,w} \nabla_\theta \ell(z_i; \hat{\theta}^*) \,. \tag{5}$$

The derivation is in Appendix A.3. To highlight, Equation 5 relies on the gradient of the *unweighted* ERM loss which is independent of w_i. Hence, the magnitude of w_i does *not* directly affect the scale of its gradient, even if $|w_i| \to 0$. Instead, w_i *indirectly* affects the gradients through the trained model parameters $\hat{\theta}^*$ and the Hessian $H_{\hat{\theta}^*,w}$. The total derivative of $\hat{\mathcal{R}}$ w.r.t. w_i is thus:

$$\frac{\mathrm{d}\hat{\mathcal{R}}(\mathcal{D}^{\text{tar}}; \hat{\theta}^*)}{\mathrm{d}w_i} = -\nabla_\theta \hat{\mathcal{R}}(\mathcal{D}^{\text{tar}}; \hat{\theta}^*)^\top H^{-1}_{\hat{\theta}^*,w} \nabla_\theta \hat{\mathcal{R}}(z_i; \hat{\theta}^*) \,. \tag{6}$$

In comparison to Equation 3, the key difference lies in the presence of the inverse Hessian term between the two gradients. The Hessian $H_{\hat{\theta}^*,w}$ describes the loss landscape of $\hat{\theta}^*$ w.r.t. the training dataset $\mathcal{D}^{\text{tr}}$ and their sample weights w. A more detailed discussion on the role of Hessian is available in Appendix C. We will show later in Section 5 that without the Hessian, the last-step approximated gradient (Equation 3) of the outer objective function is inaccurate, often leading to suboptimal results.

The derived form in Equation 6 via implicit differentiation exactly matches the influence function, which estimates the change in model parameters if a training data point z_i is upweighted infinitesimally (Cook & Weisberg, 1982; Koh & Liang, 2017). Since the influence function is well-defined for weighted objectives, we slightly generalize the notation by incorporating w into the expressions. Given a model $\hat{\theta}^*$ trained on weighted samples, the influence of upweighting $z_i \in \mathcal{D}^{\text{tr}}$ on the model predicting a target instance $z' \in \mathcal{D}^{\text{tar}}$ (or the target set $\mathcal{D}^{\text{tar}}$) is

$$\mathcal{I}(z_i, z'; \hat{\theta}^*, w) \coloneqq -\nabla_\theta \hat{\mathcal{R}}(z'; \hat{\theta}^*)^\top H^{-1}_{\hat{\theta}^*,w} \nabla_\theta \hat{\mathcal{R}}(z_i; \hat{\theta}^*) \,. \tag{7}$$

Thus, we can use the influence function to represent the gradient derived from implicit differentiation. For completeness, we define the *per-sample* influence of a dataset to be $\widetilde{\mathcal{I}}(\mathcal{D}^{\text{tr}}, z'; \hat{\theta}^*, w) \coloneqq \left[\mathcal{I}(z_1, z'; \hat{\theta}^*, w) \; \mathcal{I}(z_2, z'; \hat{\theta}^*, w) \; \cdots \; \mathcal{I}(z_n, z'; \hat{\theta}^*, w)\right]^\top \in \mathbb{R}^{n \times 1}$. Then, we can calculate the sample weight update based on the per-sample influence in $\mathcal{D}^{\text{tr}}$ on each group $g \in \mathcal{G}$ in $\mathcal{D}^{\text{tar}}$:

$$\widetilde{\mathcal{I}}(\mathcal{D}^{\text{tr}}, \mathcal{D}^{\text{tar}}_g; \hat{\theta}^*, w) = \frac{1}{|\mathcal{D}^{\text{tar}}_g|} \sum_{z' \in \mathcal{D}^{\text{tar}}_g} \widetilde{\mathcal{I}}(\mathcal{D}^{\text{tr}}, z'; \hat{\theta}^*, w) \,. \tag{8}$$

To optimize the minimax objective in the outer loop, the gradient of the worst-group risk w.r.t the sample weights can be calculated via its corresponding influence scores:

$$\frac{\mathrm{d}\hat{\mathcal{R}}^{\text{WG}}(\mathcal{D}^{\text{tar}}; \hat{\theta}^*)}{\mathrm{d}w} = \widetilde{\mathcal{I}}(\mathcal{D}^{\text{tr}}, \mathcal{D}^{\text{tar}}_{g^*}; \hat{\theta}^*, w), \quad g^* = \arg\max_{g \in \mathcal{G}} \hat{\mathcal{R}}(\mathcal{D}^{\text{tar}}_g; \hat{\theta}^*) \,. \tag{9}$$

However, only optimizing for the worst group in one step according to Equation 9 can be inefficient, especially when there are multiple groups with high error rates. To obtain a more efficient and smoother optimization trajectory, we utilize an adaptive aggregation (Sagawa et al., 2019) of the influence scores. The aggregation weights are updated multiplicatively based on the error rates among the groups to better optimize the sample weights, illustrated in lines 7-14 of Algorithm 1.

4 EXACT GROUP-ROBUST SAMPLE REWEIGHTING WITH LAST-LAYER RETRAINING

In this section, we introduce the Group-robust Sample Reweighting with last-layer retraining (GSR) algorithm. The algorithm is built on the observation that last-layer retraining (LLR) (Kang et al., 2020; Kirichenko et al., 2022) can lead to a strongly convex inner objective that satisfies the assumptions required for implicit differentiation. Next, we delineate the benefits of LLR and its integration into our GSR algorithm.

4.1 SYNERGY WITH LAST-LAYER RETRAINING

LLR is a lightweight method designed to mitigate spurious correlations and improve group robustness (Kirichenko et al., 2022; LaBonte et al., 2024; Qiu et al., 2023). In essence, it performs deep representation learning with ERM, followed by retraining only the last layer on a separate group-balanced dataset while freezing the remaining model parameters. Empirical evidence has shown that the initial ERM model has learned sufficient representations for all groups, including minority groups, and over-reliance on spurious correlations can be significantly reduced by simply fine-tuning the last linear classification layer of the model (Izmailov et al., 2022; Rosenfeld et al., 2022). As a result, despite being lightweight, last-layer retraining while freezing the ERM-learned representation has become the state-of-the-art approach for improving group robustness across various settings.

Notably, LLR synergies well with our proposed sample reweighting via implicit differentiation (Section 3), offering three significant benefits. Firstly, employing LLR with cross-entropy loss and a positive coefficient λ for ℓ_2 regularization creates a strongly convex problem that practically satisfies the Assumption 3.1 (proofs are in Appendix A.4). This allows the exact calculation of the gradients w.r.t. the sample weights via Equation 9. Secondly, calculating the Hessian inverse in Equation 6 is no longer overly expensive, because the only free model parameters are in the last layer instead of the entire deep neural network. Thirdly, LLR acts as a regularizer by limiting the capacity of the model parameters, which counterintuitively facilitates the training with weighted objectives. This is because weighted objectives do not necessarily yield different predictors compared to ERM when training overparameterized models as shown in Zhai et al. (2022). Sufficient regularization is usually needed for the reweighting scheme to be practically meaningful (Byrd & Lipton, 2019; Sagawa et al., 2019). Therefore, regularized LLR ensures that the theoretical soundness of our method translates into practical benefits without violating assumptions or conducting extensive approximations.

4.2 OUR GSR ALGORITHM

A comprehensive overview of GSR is presented in Algorithm 1. For simplicity, we omit certain details such as regularization and gradient clipping. Specifically, it contains two stages:

(Stage 1) Representation learning. We take out a random subset (e.g., 10%) from the training set as a held-out set $\mathcal{D}^{\text{tr-h}}$. Then, train the entire model θ on the remaining training set $\mathcal{D}^{\text{tr-r}}$ with ERM until convergence without early stopping. This ensures that the model fits the "remaining" training set $\mathcal{D}^{\text{tr-r}}$ well. Reserving a held-out set $\mathcal{D}^{\text{tr-h}}$ that the model has not encountered during training is a crucial step, as it prevents overfitting to the data that will be later used for sample reweighting. Otherwise, changing the sample weights will not make a meaningful difference to the last-layer classifier (Zhai et al., 2022). Note that neither group labels nor sample weights are required at this stage.

(Stage 2) Group-robust sample reweighting with last-layer retraining. Denote the model parameters as $\theta = (\phi, \psi)$ where ϕ is the feature extractor and ψ is the last-layer linear classifier. In this stage, we keep the feature extractor ϕ fixed, and jointly train the last layer ψ and the sample weights w using the held-out set $\mathcal{D}^{\text{tr-h}}$ (as a training set) and the target set $\mathcal{D}^{\text{tar}}$. Subsequently, we perform model selection with the validation set $\mathcal{D}^{\text{v}}$. We create $\mathcal{D}^{\text{tar}}$ and $\mathcal{D}^{\text{v}}$ with equal size, by

Algorithm 1 Group-robust Sample Reweighting with last-layer retraining (GSR)

Require: Training set $\mathcal{D}^{\text{tr}}$ of size n, validation set $\mathcal{D}^{\text{v}}$, target set $\mathcal{D}^{\text{tar}}$ with m groups, held-out set fraction α, outer loop steps T, outer learning rate β, scaling temperature τ.

Obtain the held-out set $\mathcal{D}^{\text{tr-h}}$ with size αn and the remaining set $\mathcal{D}^{\text{tr-r}}$ with size $(1-\alpha)n$
Stage 1:
$(\phi^*, \psi^*) \leftarrow \arg\min_{\theta=(\phi,\psi)} \hat{\mathcal{R}}(\mathcal{D}^{\text{tr-r}}; \theta)$
Stage 2:
Initialize held-out sample weights $w^{(1)} \leftarrow \frac{1}{\alpha n} \cdot \mathbf{1}^{\alpha n}$
Initialize adaptive influence score weights $\gamma^{(0)} \leftarrow \frac{1}{m} \cdot \mathbf{1}^{m}$
for $t = 1, \ldots, T$ **do**
  $\psi^{(t)} \leftarrow \arg\min_{\psi} \hat{\mathcal{R}}(\mathcal{D}^{\text{tr-h}}; w^{(t)}, (\phi^*, \psi))$ ▷ Last-layer retraining
  for $g = 1, \ldots, m$ **do**
    $\gamma_g^{(t)} \leftarrow \gamma_g^{(t-1)} \exp\left(\hat{\mathcal{R}}(\mathcal{D}_g^{\text{tar}}; (\phi^*, \psi^{(t)}))/\tau\right)$ ▷ Update aggregation weights
  end for
  $\gamma^{(t)} \leftarrow \gamma^{(t)} / \|\gamma^{(t)}\|_1$
  $\xi^{(t)} \leftarrow \mathbf{0}^{\alpha n}$
  for $g = 1, \ldots, m$ **do**
    $\xi^{(t)} = \xi^{(t)} + \gamma_g^{(t)} \widetilde{\mathcal{I}}(\mathcal{D}^{\text{tr-h}}, \mathcal{D}_g^{\text{tar}}; (\phi^*, \psi^{(t)}), w)$ ▷ Adaptive aggregation of the influence
  end for
  $w^{(t+1)} \leftarrow \max\{w^{(t)} - \beta \xi^{(t)}, \mathbf{0}^{\alpha n}\}$ ▷ Projected gradient descent (element-wise max)
  $w^{(t+1)} \leftarrow w^{(t+1)} / \|w^{(t+1)}\|_1$ ▷ Weight normalization
  if $\hat{\mathcal{R}}(\mathcal{D}^{\text{v}}; (\phi^*, \psi^{(t)})) \leq \hat{\mathcal{R}}(\mathcal{D}^{\text{v}}; (\phi^*, \psi^*))$ **then**
    $\psi^* \leftarrow \psi^{(t)}$ ▷ Model selection
  end if
end for
return $\theta^* \leftarrow (\phi^*, \psi^*)$

splitting the initial "standard" validation set in half (see remark below for the reason). The inner loop, which fits a linear classifier ψ on the weighted cross-entropy objective with ℓ_2 regularization, is optimized via L-BFGS (Liu & Nocedal, 1989) for efficiency. The outer loop performs projected gradient descent with learning rate β. The gradient is calculated using adaptive aggregation of the influence scores (Equation 9), projected to $\{w | w_i \geq 0 \, \forall i\}$. The Hessian of the inner objective is updated as $H_{\psi^{(t)}, w^{(t)}} = \nabla^2_{\psi} \hat{\mathcal{R}}(\mathcal{D}^{\text{tr-h}}; w^{(t)}, \psi^{(t)})$ in each iteration. In addition, the gradient of the sample weights can become spiky when high loss values are encountered on the validation set. We employ gradient clipping by norm and weights normalization for better training stability.

Remark. The target set and the validation set cannot be the same. Although the target data is only used to update the weights of the held-out training data and does not directly affect the training of the model parameters, overfitting to the target can still occur as a result of the representer theorem (Schölkopf et al., 2001). Thus, it is essential to create different splits for the target and validation set to prevent overfitting during sample reweighting, which we illustrate later in Figure 4d.

5 Experiments

Datasets. We evaluate the effectiveness of algorithms on 4 commonly used datasets. *Waterbirds* (Wah et al., 2011) is a binary object recognition dataset for bird types (i.e., waterbird, landbird), which are spuriously correlated with the background (i.e., water, land). *CelebA* (Liu et al., 2015) is a binary object recognition dataset for hair color blondness prediction. There exists a spurious correlation between the man gender attribute and non-blondness. *MultiNLI* (Williams et al., 2017) is a multi-class natural language inference dataset. The three classes (i.e., entailment, neutral, contradiction) describe the relationship between a pair of sentences. The spurious correlation exists between contradiction and the presence of negation words. *CivilComments (WILDS)* (Borkan et al., 2019; Koh et al., 2021) is a binary text toxicity detection dataset. There are 8 types of identities mentioned in the text, such as male and female. Grouping the samples by the identity and the class results in 16 overlapping groups. Although there are no obvious spurious correlations, the data is extremely imbalanced among

these groups, especially on text that mentions other religions and is classified as non-toxic. Overall, we follow the standard train, validation, and test splits for all datasets. We randomly create target and validation sets by equally splitting the original validation.

Baselines. We compare our approach against baselines in three categories according to the amount of group labels required. (1) Group labels for both training and validation: Group DRO (Sagawa et al., 2019) optimizes the worst-group training loss by dynamically adjusting the group weights; RWG (Idrissi et al., 2022) balances the sampling probability of each group according to their sizes. (2) Group labels for validation: JTT (Liu et al., 2021) upweights the high-loss training points that are more likely to be from minority groups. CnC (Zhang et al., 2022) in addition uses contrastive learning to align the representations of the same-class samples. SSA (Nam et al., 2022) infers the pseudo group labels of the training set by training a predictor on the validation set. DFR (Kirichenko et al., 2022) performs group-balanced last-layer retraining on the validation set. MAPLE (Zhou et al., 2022) is the most similar to ours that uses the validation set to jointly reweight the training samples and retrain the entire model. (3) No group labels required: SELF (LaBonte et al., 2024) constructs an approximately group-balanced dataset based on the disagreement from an auxiliary model, then performs class-balanced last-layer retraining. We compare against early-stop disagreement SELF, which has the best performance among its variants.

Setup. During the representation learning stage, we use the suggested hyperparameter configuration and data augmentation strategies from DFR on all datasets (with minor modifications for MultiNLI and CivilComments). At the retraining stage, we drop data augmentation and perform a randomized search of hyperparameters using the valuation set $\mathcal{D}^{\text{v}}$. The details are documented in Appendix B.2.

5.1 Improvement in group robustness

The main results are in Table 1. Our approach `GSR` achieves consistent and competitive results compared to the baseline methods in terms of group robustness, which is measured by the worst-group accuracy. Specifically, `GSR` has the state-of-the-art (SoTA) performance for both the MultiNLI and CivilComments datasets, and close-to-SoTA worst-group accuracy on the Waterbirds and CelebA datasets. Moreover, `GSR` demonstrated the highest consistency across all four datasets. It achieves an average improvement of 1.0% in absolute worst-group accuracy compared to DFR (the SoTA method which uses the same amount of group labels as ours), because `GSR` allows more fine-grained reweighting over the training data. `GSR` even outperforms Group DRO which requires more group labels, indicating that training the full network with weighted data may not always be necessary. The detailed results including the average accuracy of the methods are in Appendix B.5.

Besides, as an ablation study, we include the Hessian-free version of our method, `GSR-HF`, which uses a simplified sample weight update from MAPLE (Equation 3) during the last-layer retraining. As analyzed in Section 2 and empirically validated in Table 1, `GSR-HF` performs consistently worse than `GSR`. This highlights the importance of incorporating the Hessian matrix in Equation 6 to ensure the correctness of the gradient for adjusting the sample weights.

5.2 A closer look at sample weights

Varying weights across groups. Figure 1 illustrates the variation in the sum of sample weights across different groups through the training process of the best-performing model reported in Table 1. In general, all the minority-group weights increase, and the majority groups with spurious correlations generally have decreased weights. For example, the weights for minority groups (e.g., landbirds in water in Figure 1a) increase as optimization progresses. In contrast, the weights for certain majority groups with clear spurious correlations (e.g., landbirds on land in Figure 1a) decrease over the optimization steps. Note that not all majority groups necessarily experience a decrease in their sum of sample weights. Another key message here is that the better-performing models are not necessarily trained with equally weighted groups. In all cases, the worst-group performance is better optimized even though the groups are weighted differently, which effectively mitigates the spurious correlations with still "imbalanced" data. These results obtained from directly optimizing the sample weights align well with the similar findings in Qiu et al. (2023); Sagawa et al. (2019).

Varying weights within groups. We visualize the distribution of individual sample weights that are used to train the best models in Figure 2 (where distributions are smoothed using kernel density

Table 1: **Performance comparison.** We report the worst-group accuracy on four benchmark datasets. For the group label column, ✗ indicates no group label g is used; ✓ indicates g is required; ✓✓ indicates a proportion of g from the validation set is re-purposed beyond hyperparameter tuning, such as training sample weights or model parameters. The row sections are ranked in descending order of the total amount of group label information required. We report the mean ± standard deviation over 5 random seeds. We use "–" to indicate missing evaluation results from the original paper.

Method	Group label Train / Val	Worst-group accuracy (%) Waterbirds	CelebA	MultiNLI	CivilComments	Average
Group DRO	✓/ ✓	$91.4_{\pm 1.1}$	$88.9_{\pm 2.3}$	$77.7_{\pm 1.4}$	$70.0_{\pm 2.0}$	82.0
RWG	✓/ ✓	$87.6_{\pm 1.6}$	$84.3_{\pm 1.8}$	$69.6_{\pm 1.0}$	$72.0_{\pm 1.9}$	78.4
JTT	✗/ ✓	86.7	81.1	72.6	69.3	77.4
CnC	✗/ ✓	$88.5_{\pm 0.3}$	$88.8_{\pm 0.9}$	–	$68.9_{\pm 2.1}$	–
SSA	✗/ ✓✓	$89.0_{\pm 0.6}$	$\mathbf{89.8}_{\pm 1.3}$	$76.6_{\pm 0.7}$	$69.9_{\pm 2.0}$	81.3
MAPLE	✗/ ✓✓	91.7	88.0	72.7	64.1	79.1
DFR	✗/ ✓✓	$\mathbf{92.9}_{\pm 0.2}$	$88.3_{\pm 1.1}$	$74.7_{\pm 0.7}$	$70.1_{\pm 0.8}$	81.5
GSR−HF	✗/ ✓✓	$87.5_{\pm 0.1}$	$86.3_{\pm 0.4}$	$74.7_{\pm 0.0}$	$68.9_{\pm 0.2}$	79.4
GSR	✗/ ✓✓	$\mathbf{92.9}_{\pm 0.0}$	$87.0_{\pm 0.4}$	$\mathbf{78.5}_{\pm 0.3}$	$\mathbf{71.7}_{\pm 0.6}$	**82.5**
ERM	✗/ ✗	$74.9_{\pm 2.4}$	$46.9_{\pm 2.8}$	$65.9_{\pm 0.3}$	$55.6_{\pm 0.6}$	60.8
SELF	✗/ ✗	$\mathbf{93.0}_{\pm 0.3}$	$83.9_{\pm 0.9}$	$70.7_{\pm 2.5}$	–	–

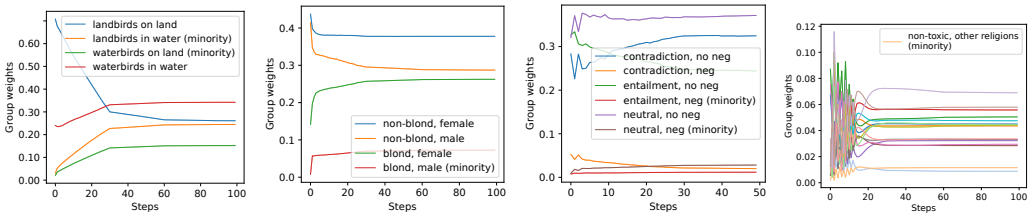

(a) Waterbirds (b) CelebA (c) MNLI (d) CivilComments

Figure 1: The change in the sum of sample weights across different groups throughout the training. The minority groups are upweighted and the majority groups are generally downweighted. However, different groups do not have equal sums of weights.

estimation). The samples from the majority groups are consistently assigned with lower weights after reweighting, especially for Waterbirds and CelebA in Figures 2a, 2b. On the other hand, the minority groups are consistently upweighted with their sample weights stretched out to larger values across all datasets. We can also clearly see that our best-performing models are trained on samples with diverse weights, even if they are from the same group. This implies that not all samples need to be upweighted or downweighted for group-balanced training. Having more fine-grained adjustments over the sample weights offers more flexibility in improving the robustness to subpopulation shifts.

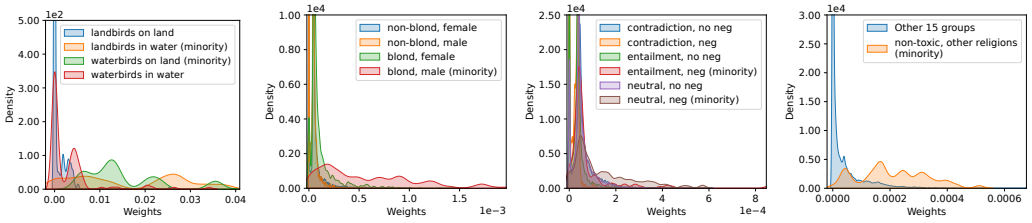

(a) Waterbirds (b) CelebA (c) MNLI (d) CivilComments

Figure 2: The distribution of sample weights for each group that are used to train the best models. The minority groups have the weight distribution stretched out towards high values, while the majority-group weights are generally skewed towards 0.

Visualizing high-weight samples. In addition, we visualize the held-out samples with the highest weight from Waterbirds in Figure 3. These high-weight samples also tend to be consistent across different runs. All of these images are from the minority groups (waterbirds on land, landbirds in water). As highlighted by the red box, the image has a background that arguably resembles more land than water. Hence, it should be considered as a minority. Since the group labels for the held-out sets are not used for retraining, GSR is not affected by the annotation errors for group labels and correctly assigns high weights to these samples, since they are supposedly helpful in improving the worst-group performance in the high-quality target set. However, other group-balanced baselines that directly train on these group labels do not offer such a benefit. We will subsequently show that GSR is robust to class-label errors in the training data in Section 5.3.

(a) The *most* weighted instances. (b) The *least* weighted instances.

Figure 3: We illustrate the selected images with their class label and background label from the held-out split in Waterbirds according to the sample weights. In 3a, the top-5 highest weighted instances are all from the minority groups with differing bird types and backgrounds. As highlighted in the red box in (a), the background of the waterbird is arguably closer to land than water and hence should be categorized as a minority. GSR is able to correctly identify them even though they have wrong annotations. In 3b, the top-5 lowest weighted instances are all from the majority groups where the background is spuriously correlated with the bird type.

5.3 Robustness to Label Noise

The real-world data often have annotation errors (Beyer et al., 2020; Gururangan et al., 2018). Assuming efforts are invested into the quality of the group-labeled dataset $\mathcal{D}^{\mathrm{L}}$, the other training data without group labels in $\mathcal{D}^{\mathrm{U}}$ may have unaddressed errors such as mislabeled classes. To evaluate the resilience of GSR on training data with different quality, we simulate the variation of data quality by adding class label noise. In particular, we randomly flip up to 40% of the class labels in the held-out set to incorrect classes, and leave the target and validation sets unchanged. As shown in Figure 4a, the worst-group performance of GSR has minimal performance degradation. This is because using high-quality targets for training sample reweighting allows more fine-grained control over the training data. To further understand why, we plot the learned weight distribution of the held-out data in Waterbirds. Compared to that of the clean data in Figure 4b, the weight distribution of the noisy data is more skewed towards 0 as shown in Figure 4c. In particular, almost all minority instances with noisy labels have close-to-0 weights, equivalent to being removed from the training set. Therefore, the efficacy of GSR can be attributed to the property of automatically "cleaning" the training data

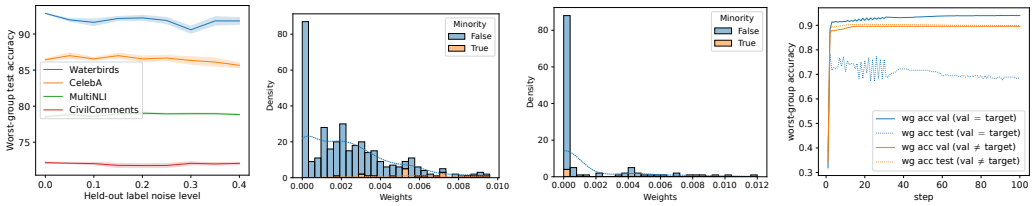

(a) Label noise robustness (b) Clean data weights (c) Noisy data weights (d) Val vs. test acc

Figure 4: In-depth study of our algorithm. In 4a, the worst-group test accuracy degrades slightly even when up to 40% of the held-out set labels are corrupted. In 4b, most of the uncorrupted minority samples received higher weight assignments than non-minority examples. In contrast, in 4c, the corrupted minority instances are correctly assigned with close-to-0 weights. 4d shows the relationship between validation and test worst-group accuracy on the CelebA dataset. It is important to have separate target and validation sets. Otherwise, overfitting can easily occur.

via sample reweighting. GSR being robust to class label corruption has an important implication: to improve the robustness to distribution shifts under a limited annotation budget, more efforts should be dedicated to ensuring the quality of the target set.

6 Related Work

Subpopulation shifts. Group labels are essential for training and evaluating machine learning models under subpopulation shifts. Various approaches have been proposed to handle scenarios with different levels of availability of group labels: fully known for all data splits (Deng et al., 2024; Idrissi et al., 2022; Sagawa et al., 2019), partially known (Kirichenko et al., 2022; Liu et al., 2021; 2022; Nam et al., 2022; Qiu et al., 2023; Zhang et al., 2022; Zhou et al., 2022), or completely unknown (Han & Zou, 2024; LaBonte et al., 2024). In addition, Yang et al. (2023) comprehensively studied the effectiveness of these approaches on a variety of benchmarks with unknown group labels and demonstrated that optimizing for the worst class can be surprisingly effective for improving the worst-group performance. Our approach falls into the category of learning with partial group labels (from the validation set) and differs from most of the approaches by using group-labeled data for sample reweighting instead of direct training.

Sample reweighting and implicit differentiation. Optimizing sample weights jointly with the model parameters is useful for robust deep learning (Ren et al., 2018) and group robustness (Zhou et al., 2022). These works focus on using truncated backpropagation to circumvent the challenge of differentiating through the unrolled training trajectory. Implicit differentiation is an alternative solution to the problem and has been applied to areas such as hyperparameter optimization (Foo et al., 2007; Lorraine et al., 2020; Pedregosa, 2016), meta-learning (Lee et al., 2019; Rajeswaran et al., 2019), generative modeling (Domke, 2012; Samuel & Tappen, 2009), and fairness (Shui et al., 2022). In addition, Li & Liu (2022); Wang et al. (2024) have explored one-step (i.e., not iterative) sample reweighting via the influence function for algorithmic fairness. Bae et al. (2022) shows an alternative derivation of the influence function via implicit differentiation on the training set. In contrast to these works, we show the connection between the influence function and bilevel optimization via implicit differentiation and devise an efficient scheme to rigorously apply it iteratively for addressing subpopulation shifts.

7 Conclusion and Future Work

Motivated from the bilevel minimax objective, GSR utilizes the group-labeled data for fine-grained reweighting of the training samples via a soft aggregation of the influence functions. It seamlessly integrates with last-layer retraining, resulting in a lightweight and effective strategy for improving group robustness. GSR also has the ability to automatically clean and guide the training of potentially noisy datasets via sample reweighting. Our deeper dive into the empirical analysis further supports the alternative training paradigm that emphasizes the use of high-quality, group-labeled instances as the target set.

We also identify several directions for future work to further improve our method. Despite GSR achieving competitive worst-group performance, it usually results in a decrease in mean performance. This practical trade-off is commonly seen in efforts to improve group robustness (Chen et al., 2022). We note that sample reweighting offers an alternative way to test the limit of last-layer retraining, however, it does not improve the representation learning. To mitigate the trade-off between the worst-group and the mean performance, enhancing the quality of representations is still a critical step (Izmailov et al., 2022).

Additionally, our work is based on the hypothesis that standard ERM learns sufficiently high-quality representations. However, this assumption may not always hold, particularly under certain subpopulation shifts (Yang et al., 2023). The question of whether sample reweighting can improve the representation learning for the group robustness remains unanswered, which necessitates retraining more components of the model after obtaining the sample weights. Developing more efficient strategies that jointly optimize the sample weights and deep model parameters may offer more insights and advancements in tackling subpopulation shifts and beyond.

REFERENCES

Naman Agarwal, Brian Bullins, and Elad Hazan. Second-order stochastic optimization for machine learning in linear time. *Journal of Machine Learning Research*, 18(116):1–40, 2017.

Martin Arjovsky, Léon Bottou, Ishaan Gulrajani, and David Lopez-Paz. Invariant risk minimization. *arXiv preprint arXiv:1907.02893*, 2019.

Juhan Bae, Nathan Ng, Alston Lo, Marzyeh Ghassemi, and Roger B Grosse. If influence functions are the answer, then what is the question? *Advances in Neural Information Processing Systems*, 35:17953–17967, 2022.

Lucas Beyer, Olivier J Hénaff, Alexander Kolesnikov, Xiaohua Zhai, and Aäron van den Oord. Are we done with imagenet? *arXiv preprint arXiv:2006.07159*, 2020.

Daniel Borkan, Lucas Dixon, Jeffrey Sorensen, Nithum Thain, and Lucy Vasserman. Nuanced metrics for measuring unintended bias with real data for text classification. In *Companion Proceedings of the 2019 World Wide Web Conference*, pp. 491–500, 2019.

Stephen Boyd and Lieven Vandenberghe. *Convex optimization*. Cambridge University Press, 2004.

Jonathon Byrd and Zachary Lipton. What is the effect of importance weighting in deep learning? In *International Conference on Machine Learning*, pp. 872–881, 2019.

Yongqiang Chen, Kaiwen Zhou, Yatao Bian, Binghui Xie, Bingzhe Wu, Yonggang Zhang, Kaili Ma, Han Yang, Peilin Zhao, Bo Han, et al. Pareto invariant risk minimization: Towards mitigating the optimization dilemma in out-of-distribution generalization. *arXiv preprint arXiv:2206.07766*, 2022.

R Dennis Cook and Sanford Weisberg. Residuals and influence in regression, 1982.

Yihe Deng, Yu Yang, Baharan Mirzasoleiman, and Quanquan Gu. Robust learning with progressive data expansion against spurious correlation. In *Advances in Neural Information Processing Systems*, volume 36, 2024.

Justin Domke. Generic methods for optimization-based modeling. In *International Conference on Artificial Intelligence and Statistics*, pp. 318–326. PMLR, 2012.

Cynthia Dwork, Moritz Hardt, Toniann Pitassi, Omer Reingold, and Richard Zemel. Fairness through awareness. In *Proceedings of the 3rd Innovations in Theoretical Computer Science Conference*, pp. 214–226, 2012.

Chuan-sheng Foo, Chuong B., and Andrew Ng. Efficient multiple hyperparameter learning for log-linear models. In *Advances in Neural Information Processing Systems*, volume 20, 2007.

Robert Geirhos, Jörn-Henrik Jacobsen, Claudio Michaelis, Richard Zemel, Wieland Brendel, Matthias Bethge, and Felix A Wichmann. Shortcut learning in deep neural networks. In *Nature Machine Intelligence*, volume 2, pp. 665–673. Nature Publishing Group UK London, 2020.

Suchin Gururangan, Swabha Swayamdipta, Omer Levy, Roy Schwartz, Samuel R Bowman, and Noah A Smith. Annotation artifacts in natural language inference data. *arXiv preprint arXiv:1803.02324*, 2018.

Yujin Han and Difan Zou. Improving group robustness on spurious correlation requires preciser group inference. *arXiv preprint arXiv:2404.13815*, 2024.

Kaiming He, Xiangyu Zhang, Shaoqing Ren, and Jian Sun. Deep residual learning for image recognition. In *Proceedings of the IEEE/CVF Conference on Computer Vision and Pattern Recognition*, pp. 770–778, 2016.

Katherine L Hermann, Hossein Mobahi, Thomas Fel, and Michael C Mozer. On the foundations of shortcut learning. In *International Conference on Learning Representations*, 2024.

Badr Youbi Idrissi, Martin Arjovsky, Mohammad Pezeshki, and David Lopez-Paz. Simple data balancing achieves competitive worst-group-accuracy. In *Conference on Causal Learning and Reasoning*, pp. 336–351. PMLR, 2022.

Pavel Izmailov, Polina Kirichenko, Nate Gruver, and Andrew G Wilson. On feature learning in the presence of spurious correlations. In *Advances in Neural Information Processing Systems*, pp. 38516–38532, 2022.

Bingyi Kang, Saining Xie, Marcus Rohrbach, Zhicheng Yan, Albert Gordo, Jiashi Feng, and Yannis Kalantidis. Decoupling representation and classifier for long-tailed recognition. In *International Conference on Learning Representations*, 2020.

Polina Kirichenko, Pavel Izmailov, and Andrew Gordon Wilson. Last layer re-training is sufficient for robustness to spurious correlations. *arXiv preprint arXiv:2204.02937*, 2022.

Pang Wei Koh and Percy Liang. Understanding black-box predictions via influence functions. In *International Conference on Machine Learning*, pp. 1885–1894. PMLR, 2017.

Pang Wei Koh, Shiori Sagawa, Henrik Marklund, Sang Michael Xie, Marvin Zhang, Akshay Balsubramani, Weihua Hu, Michihiro Yasunaga, Richard Lanas Phillips, Irena Gao, et al. Wilds: A benchmark of in-the-wild distribution shifts. In *International Conference on Machine Learning*, pp. 5637–5664, 2021.

Steven George Krantz and Harold R Parks. *The implicit function theorem: history, theory, and applications*. Springer Science & Business Media, 2002.

Tyler LaBonte, Vidya Muthukumar, and Abhishek Kumar. Towards last-layer retraining for group robustness with fewer annotations. In *Advances in Neural Information Processing Systems*, volume 36, 2024.

Kwonjoon Lee, Subhransu Maji, Avinash Ravichandran, and Stefano Soatto. Meta-learning with differentiable convex optimization. In *Proceedings of the IEEE/CVF Conference on Computer Vision and Pattern Recognition*, pp. 10657–10665, 2019.

Peizhao Li and Hongfu Liu. Achieving fairness at no utility cost via data reweighing with influence. In *International Conference on Machine Learning*, pp. 12917–12930. PMLR, 2022.

Weixin Liang and James Zou. Metashift: A dataset of datasets for evaluating contextual distribution shifts and training conflicts. *arXiv preprint arXiv:2202.06523*, 2022.

Dong C Liu and Jorge Nocedal. On the limited memory bfgs method for large scale optimization. *Mathematical programming*, 45(1):503–528, 1989.

Evan Z Liu, Behzad Haghgoo, Annie S Chen, Aditi Raghunathan, Pang Wei Koh, Shiori Sagawa, Percy Liang, and Chelsea Finn. Just train twice: Improving group robustness without training group information. In *International Conference on Machine Learning*, pp. 6781–6792, 2021.

Sheng Liu, Xu Zhang, Nitesh Sekhar, Yue Wu, Prateek Singhal, and Carlos Fernandez-Granda. Avoiding spurious correlations via logit correction. *arXiv preprint arXiv:2212.01433*, 2022.

Ziwei Liu, Ping Luo, Xiaogang Wang, and Xiaoou Tang. Deep learning face attributes in the wild. In *Proceedings of the IEEE International Conference on Computer Vision*, pp. 3730–3738, 2015.

Jonathan Lorraine, Paul Vicol, and David Duvenaud. Optimizing millions of hyperparameters by implicit differentiation. In *International Conference on Artificial Intelligence and Statistics*, pp. 1540–1552. PMLR, 2020.

Vaishnavh Nagarajan, Anders Andreassen, and Behnam Neyshabur. Understanding the failure modes of out-of-distribution generalization. *arXiv preprint arXiv:2010.15775*, 2020.

Junhyun Nam, Jaehyung Kim, Jaeho Lee, and Jinwoo Shin. Spread spurious attribute: Improving worst-group accuracy with spurious attribute estimation. *arXiv preprint arXiv:2204.02070*, 2022.

Fabian Pedregosa. Hyperparameter optimization with approximate gradient. In *International Conference on Machine Learning*, pp. 737–746. PMLR, 2016.

Geoff Pleiss, Tianyi Zhang, Ethan Elenberg, and Kilian Q Weinberger. Identifying mislabeled data using the area under the margin ranking. In *Advances in Neural Information Processing Systems*, volume 33, pp. 17044–17056, 2020.

Shikai Qiu, Andres Potapczynski, Pavel Izmailov, and Andrew Gordon Wilson. Simple and fast group robustness by automatic feature reweighting. In *International Conference on Machine Learning*, pp. 28448–28467. PMLR, 2023.

Aravind Rajeswaran, Chelsea Finn, Sham M Kakade, and Sergey Levine. Meta-learning with implicit gradients. In *Advances in Neural Information Processing Systems*, volume 32, 2019.

Mengye Ren, Wenyuan Zeng, Bin Yang, and Raquel Urtasun. Learning to reweight examples for robust deep learning. In *International Conference on Machine Learning*, pp. 4334–4343. PMLR, 2018.

Elan Rosenfeld, Pradeep Ravikumar, and Andrej Risteski. Domain-adjusted regression or: ERM may already learn features sufficient for out-of-distribution generalization. *arXiv preprint arXiv:2202.06856*, 2022.

Shiori Sagawa, Pang Wei Koh, Tatsunori B Hashimoto, and Percy Liang. Distributionally robust neural networks for group shifts: On the importance of regularization for worst-case generalization. *arXiv preprint arXiv:1911.08731*, 2019.

Shiori Sagawa, Aditi Raghunathan, Pang Wei Koh, and Percy Liang. An investigation of why overparameterization exacerbates spurious correlations. *arXiv preprint arXiv:2005.04345*, 2020.

Kegan G. G. Samuel and Marshall F. Tappen. Learning optimized MAP estimates in continuously-valued mrf models. In *Proceedings of the IEEE/CVF Conference on Computer Vision and Pattern Recognition*, pp. 477–484, 2009.

Bernhard Schölkopf, Ralf Herbrich, and Alex J Smola. A generalized representer theorem. In *International Conference on Computational Learning Theory*, pp. 416–426. Springer, 2001.

Amirreza Shaban, Ching-An Cheng, Nathan Hatch, and Byron Boots. Truncated back-propagation for bilevel optimization. In *International Conference on Artificial Intelligence and Statistics*, pp. 1723–1732. PMLR, 2019.

Harshay Shah, Kaustav Tamuly, Aditi Raghunathan, Prateek Jain, and Praneeth Netrapalli. The pitfalls of simplicity bias in neural networks. In *Advances in Neural Information Processing Systems*, pp. 9573–9585, 2020.

Changjian Shui, Qi Chen, Jiaqi Li, Boyu Wang, and Christian Gagné. Fair representation learning through implicit path alignment. In *International Conference on Machine Learning*, pp. 20156–20175. PMLR, 2022.

Swabha Swayamdipta, Roy Schwartz, Nicholas Lourie, Yizhong Wang, Hannaneh Hajishirzi, Noah A Smith, and Yejin Choi. Dataset cartography: Mapping and diagnosing datasets with training dynamics. *arXiv preprint arXiv:2009.10795*, 2020.

C. Wah, S.Branson, P. Welinder, P. Perona, and S. Belongie. The caltech-ucsd birds-200-2011 dataset. *California Institute of Technology*, 2011.

Haonan Wang, Ziwei Wu, and Jingrui He. Fairif: Boosting fairness in deep learning via influence functions with validation set sensitive attributes. In *Proceedings of the ACM International Conference on Web Search and Data Mining*, pp. 721–730, 2024.

Adina Williams, Nikita Nangia, and Samuel R Bowman. A broad-coverage challenge corpus for sentence understanding through inference. *arXiv preprint arXiv:1704.05426*, 2017.

Yuzhe Yang, Haoran Zhang, Dina Katabi, and Marzyeh Ghassemi. Change is hard: A closer look at subpopulation shift. In *International Conference on Machine Learning*, 2023.

Bianca Zadrozny. Learning and evaluating classifiers under sample selection bias. In *International Conference on Machine Learning*, pp. 114, 2004.

Runtian Zhai, Chen Dan, Zico Kolter, and Pradeep Ravikumar. Understanding why generalized reweighting does not improve over ERM. *arXiv preprint arXiv:2201.12293*, 2022.

Michael Zhang, Nimit S Sohoni, Hongyang R Zhang, Chelsea Finn, and Christopher Ré. Correct-n-contrast: A contrastive approach for improving robustness to spurious correlations. *arXiv preprint arXiv:2203.01517*, 2022.

Xiao Zhou, Yong Lin, Renjie Pi, Weizhong Zhang, Renzhe Xu, Peng Cui, and Tong Zhang. Model agnostic sample reweighting for out-of-distribution learning. In *International Conference on Machine Learning*, pp. 27203–27221. PMLR, 2022.

A Derivations and Proofs

A.1 Derivation of the Jacobian of the gradient w.r.t. the sample weights

The derivative of $\nabla_\theta \hat{\mathcal{R}}(\mathcal{D}^{\text{tr}}; w, \theta)$ w.r.t. individual sample weights w_i is:

$$\begin{aligned}
\nabla_{w_i} \nabla_\theta \hat{\mathcal{R}}(\mathcal{D}^{\text{tr}}; w, \theta) &= \nabla_{w_i} \nabla_\theta \sum_{j \in 1,\dots,|\mathcal{D}^{\text{tr}}|} w_j \ell(x_j^{\text{tr}}, y_j^{\text{tr}}; \theta) \\
&= \nabla_{w_i} \sum_{j \in 1,\dots,|\mathcal{D}^{\text{tr}}|} w_j \nabla_\theta \ell(x_j^{\text{tr}}, y_j^{\text{tr}}; \theta) \\
&= \nabla_\theta \ell(x_i^{\text{tr}}, y_i^{\text{tr}}; \theta) \\
&= \nabla_\theta \hat{\mathcal{R}}(z_i; \theta_T) \qquad (10)
\end{aligned}$$

A.2 Derivation of last-step gradient (MAPLE (Zhou et al., 2022))

According to MAPLE's one-step truncated backpropagation, the gradient descent updates before θ_{T-1} are truncated, so that θ_{T-1} is a "constant" and is independent of w. Thus, it is true that $\nabla_{w_i} \theta_{T-1} = 0$, but not for $\nabla_{w_i} \theta_T$. Recall that for simplicity, we use the notation $\nabla_\theta \hat{\mathcal{R}}(\mathcal{D}^{\text{tr}}; w, \theta_T)$ for $\nabla_\theta \hat{\mathcal{R}}(\mathcal{D}^{\text{tr}}; w, \theta)\Big|_{\theta=\theta_T}$. We show that Equation 2 can be derived as follows:

$$\begin{aligned}
\nabla_{w_i} \hat{\theta}^* &\approx \nabla_{w_i} \theta_T \\
&\approx \nabla_{w_i} \left(\theta_{T-1} - \eta \nabla_\theta \hat{\mathcal{R}}(\mathcal{D}^{\text{tr}}; w, \theta_{T-1}) \right) && \text{(One-step truncation)} \\
&\approx \nabla_{w_i} \left(\theta_{T-1} - \eta \nabla_\theta \hat{\mathcal{R}}(\mathcal{D}^{\text{tr}}; w, \theta_T) \right) \\
&\qquad (\theta_T \approx \theta_{T-1} \text{ on convergence, so } \nabla_\theta \hat{\mathcal{R}}(\mathcal{D}^{\text{tr}}; w, \theta_T) \approx \nabla_\theta \hat{\mathcal{R}}(\mathcal{D}^{\text{tr}}; w, \theta_{T-1})) \\
&= 0 - \eta \nabla_{w_i} \nabla_\theta \hat{\mathcal{R}}(\mathcal{D}^{\text{tr}}; w, \theta_T) && (\nabla_{w_i} \theta_{T-1} = 0 \text{ because of one-step truncation}) \\
&= -\eta \nabla_\theta \hat{\mathcal{R}}(z_i; \theta_T) && \text{(Apply Equation 10)}
\end{aligned}$$

A.3 Derivation of meta-gradient update

We utilize the technique of implicit differentiation. Upon convergence to an optimal solution, the inner problem has the property of $\nabla_\theta \hat{\mathcal{R}}(\mathcal{D}^{\text{tr}}; w, \hat{\theta}^*) = 0$. By first differentiating w.r.t. w on both sides of the equation, then followed by the chain rule, we have the following derivations:

$$\begin{aligned}
\frac{\mathrm{d}0}{\mathrm{d}w} &= \frac{\mathrm{d}\nabla_\theta \hat{\mathcal{R}}(\mathcal{D}^{\text{tr}}; w, \hat{\theta}^*)}{\mathrm{d}w} \\
0 &= \frac{\mathrm{d}\nabla_\theta \hat{\mathcal{R}}(\mathcal{D}^{\text{tr}}; w, \hat{\theta}^*)}{\mathrm{d}w} \\
0 &= \frac{\partial \nabla_\theta \hat{\mathcal{R}}(\mathcal{D}^{\text{tr}}; w, \hat{\theta}^*)}{\partial w} + \frac{\partial \nabla_\theta \hat{\mathcal{R}}(\mathcal{D}^{\text{tr}}; w, \hat{\theta}^*)}{\partial \hat{\theta}^*} \frac{\mathrm{d}\hat{\theta}^*}{\mathrm{d}w} && \text{(Chain-rule)} \\
0 &= \nabla_w \nabla_\theta \hat{\mathcal{R}}(\mathcal{D}^{\text{tr}}; w, \hat{\theta}^*) + \nabla_\theta^2 \hat{\mathcal{R}}(\mathcal{D}^{\text{tr}}; w, \hat{\theta}^*) \frac{\mathrm{d}\hat{\theta}^*}{\mathrm{d}w} \\
\frac{\mathrm{d}\hat{\theta}^*}{\mathrm{d}w} &= -\left(\nabla_\theta^2 \hat{\mathcal{R}}(\mathcal{D}^{\text{tr}}; w, \hat{\theta}^*) \right)^{-1} \nabla_w \nabla_\theta \hat{\mathcal{R}}(\mathcal{D}^{\text{tr}}; w, \hat{\theta}^*) \\
\frac{\mathrm{d}\hat{\theta}^*}{\mathrm{d}w} &= -H_{\hat{\theta}^*, w}^{-1} \nabla_w \nabla_\theta \hat{\mathcal{R}}(\mathcal{D}^{\text{tr}}; w, \hat{\theta}^*)
\end{aligned}$$

For each sample weight w_i:

$$\begin{aligned}
\frac{\mathrm{d}\hat{\theta}^*}{\mathrm{d}w_i} &= -H_{\hat{\theta}^*, w}^{-1} \nabla_{w_i} \nabla_\theta \hat{\mathcal{R}}(\mathcal{D}^{\text{tr}}; w, \hat{\theta}^*) \\
&= -H_{\hat{\theta}^*, w}^{-1} \hat{\mathcal{R}}(z_i; \theta_T) && \text{(Apply Equation 10)}
\end{aligned}$$

A.4 Proof of the Strong Convexity of Linear Classification with Cross-entropy Loss and ℓ_2-Regularization

In this section, we add the complete proof for the established result of the strong convexity of linear classification with cross-entropy loss and ℓ_2-regularization. Before introducing the complete proof, a shortcut intuitive proof for this consists of the following steps:

1. Linear classification with cross-entropy loss is convex, and its Hessian H is positive semi-definite, implying $H \succeq 0$.
2. Adding ℓ_2-regularization with a positive regularization strength $\lambda > 0$ produces a new Hessian $H' = H + \lambda I \succeq \lambda I$, which meets the definition of strong convexity (Definition A.1).

We now present a complete proof of the result of the strong convexity by directly showing the H' in Theorem A.6.

Definition A.1 (μ-Strong convexity (Boyd & Vandenberghe, 2004))**.** For $\mu > 0$, a differentiable function f is μ-strongly convex if for some $\mu > 0$, $\nabla^2 f(x) \succeq \mu I$.

Definition A.2 (One-hot Vector)**.** For a dimension d, $u(i) \in \{0,1\}^d, \sum u(i) = 1$ is the one-hot vector with i-th dimension $u(i)_i = 1$. We omit d in the following context for simplicity.

Definition A.3 (Softmax)**.** Given the input $x \in \mathbb{R}^d$, define the softmax function $\sigma : \mathbb{R}^d \to \mathbb{R}^d$ as:

$$\sigma(x)_i = \frac{e^{x_i}}{\sum_i e^{x_i}} .$$

Its derivative $\nabla_x \sigma(x) \in \mathbb{R}^{d \times d}$ has the form:

$$\nabla_x \sigma(x) = \operatorname{diag}(\sigma(x)) - \sigma(x)\sigma(x)^\top . \tag{11}$$

In addition,

$$\nabla_x \sigma(x)_i = \sigma(x)_i (u(i) - \sigma(x)) , \tag{12}$$

where $u(i) \in \{0,1\}^d, \sum u(i) = 1$ is the one-hot vector with i-th dimension $u(i)_i = 1$.

Proposition A.4. *The first-order derivative matrix $\nabla_x \sigma(x)$ of the softmax function is positive semidefinite.*

Proof. First $\sigma(x)$ defines a probability distribution. Hence, it has the property that $\sigma(x)_i \geq 0 \; \forall i, \; \sum_i \sigma(x)_i = 1$. Then according to the definition of positive semidefiniteness: $\forall z \in \mathbb{R}^d, z \neq \mathbf{0}$:

$$\begin{aligned} z^\top \nabla_x \sigma(x) z &= z^\top (\operatorname{diag}(\sigma(x)) - \sigma(x)\sigma(x)^\top) z \\ &= z^\top \operatorname{diag}(\sigma(x)) z - z^\top \sigma(x)\sigma(x)^\top z \\ &= \sum_i \sigma(x)_i z_i^2 - (\sum_i \sigma(x)_i z_i)^2 \\ &\geq 0 . \qquad \text{(Cauchy-Schwartz)} \end{aligned}$$

□

Definition A.5 (Cross-entropy)**.** Given the input $z \in \mathbb{R}^d, y \in \{1, \ldots, K\}$ for a K-way classification problem, define the cross entropy loss L:

$$\mathrm{CE}(z, y) = -\sum_k^K \mathbb{I}[y = k] \log z_i ,$$

where $\mathbb{I}$ is the indicator function.

Theorem A.6 (Strong convexity of cross-entropy loss with ℓ_2-regularization)**.** *For multi-class linear classification with cross-entropy loss, if ℓ_2-regularization with positive coefficient λ is applied, then the objective is λ-strongly convex.*

Proof. Let $x \in \mathbb{R}, y \in \{1, \dots, K\}$ denote the input, label of a K-way classification task. Let $\psi \in \mathbb{R}^{d \times K}$ denote the linear model parameters. Let $u(y)$ denote the one-hot representation of y. The objective function using cross-entropy loss and ℓ_2-regularization is:

$$\begin{aligned} L(x, y; \psi) &= \mathrm{CE}(\sigma(\psi^\top x), y) + \frac{\lambda}{2}\|\psi\|_2^2 \\ &= -\sum_k^K \mathbb{I}[y = k] \log\big(\sigma(\psi^\top x)_k\big) + \frac{\lambda}{2}\|\psi\|_2^2 \\ &= -\log\big(\sigma(\psi^\top x)_y\big) + \frac{\lambda}{2}\|\psi\|_2^2 \,. \end{aligned}$$

The first-order derivative:

$$\begin{aligned} \nabla_\psi L(x, y; \psi) &= -x\frac{1}{\sigma(\psi^\top x)_y}\sigma(\psi^\top x)_y \left(u(y) - \sigma(\psi^\top x)\right)^\top + \lambda\psi && \text{(Equation 12)} \\ &= x(\sigma(\psi^\top x) - u(y))^\top + \lambda\psi \,. \end{aligned}$$

The second-order derivative (Hessian):

$$\begin{aligned} H &= \nabla_\psi^2 L(x, y; \psi) \\ &= \frac{\partial x(\sigma(\psi^\top x) - u(y))^\top}{\partial \psi} + \lambda I_{d\times k} \\ &= x\frac{\partial \sigma(\psi^\top x)^\top}{\partial \psi} + \lambda I_{d\times k} \\ &= x(x(\mathrm{diag}(\sigma(x)) - \sigma(x)\sigma(x)^\top))^\top + \lambda I_{d\times k} && \text{(Equation 11)} \\ &= x\left(\mathrm{diag}(\sigma(x)) - \sigma(x)\sigma(x)^\top\right)x^\top + \lambda I_{d\times k} \,. \end{aligned}$$

Then we show that the Hessian of L meets the requirement of λ-strong convexity, i.e., $H - \lambda I \succeq 0$, $\forall z \in \mathbb{R}^{d\times k}, z \neq 0$:

$$\begin{aligned} z^\top(H - \lambda I_{d\times k})z &= z^\top x\left(\mathrm{diag}(\sigma(x)) - \sigma(x)\sigma(x)^\top\right)x^\top z + z^\top(\lambda I_{d\times k} - \lambda I_{d\times k})z \\ &= z^\top x\left(\mathrm{diag}(\sigma(x)) - \sigma(x)\sigma(x)^\top\right)x^\top z \\ &\geq 0 \,. && \text{(Proposition A.4)} \end{aligned}$$

Hence, L is strongly convex according to Definition A.1. □

B Experimental Details

B.1 Setup

For model architectures and initialization, we use ImageNet-pretrained ResNet-50 (V1) (He et al., 2016) for Waterbirds and CelebA datasets, and use BERT (HuggingFace) for MultiNLI and CivilComments. The MNLI dataset is preprocessed according to the setup in `https://github.com/kohpangwei/group_DROBertTokenizer`. The CivilComment dataset is tokenized with BertTokenizer with max_seq_length=300. For all experiments, we perform 5 independent runs on seed [1, 2, 3, 4, 5] to obtain the mean and the standard deviations.

B.2 Hyperparameters

For all experiments, we fix the held-out fraction α as 10% and the resulting partition splits (i.e., the held-out set and the remaining set) of the training set $\mathcal{D}^{\text{tr}}$, which are generated by fixed numpy random seed 1. Although it is true that additionally tuning the held-out fraction α and changing the split can most likely improve the worst-group performance by balancing the data for representation

learning and sample reweighting, we do not alter these splits for better consistency and focus only on the second sample reweighting stage of the training.

For stage 1, we use *almost* the same hyperparameters as used by DFR (some are slightly altered for better consistency and simplicity by heuristics without tuning) and record them in Table 2.

For stage 2, there are two sets of hyperparameters for the inner and the outer loop. We perform a non-exhaustive search by randomly sampling the combination of hyperparameters from the grid. We select the best-performing model and hyperparameter configurations based on the worst-group validation accuracy. The selected hyperparameter configurations are documented in Tables 4 and 3 for the inner and the outer loop respectively. Besides, we consistently apply weight normalization (to ensure the sum of weights equals to one) and a step learning rate scheduler (StepLR), which decays the outer learning rate by a factor of 10 every 30 steps without tuning.

Table 2: **Hyperparameters for base model training**. For Waterbirds and CelebA, we use *almost* the same hyperparameters as used by DFR. We slightly change the hyperparameters on MNLI and CivilComments (without any tuning) so that no learning rate scheduler is used. Momentum is set as 0.9 for SGD.

Dataset	optimizer	lr	scheduler	batch size	weight decay	epochs
Waterbirds	SGD	1e-3	Constant	32	1e-3	100
CelebA	SGD	1e-3	Constant	128	1e-4	50
MultiNLI	AdamW	2e-5	Constant	32	1e-4	4
CivilComments	AdamW	2e-5	Constant	32	1e-4	4

Table 3: Hyperparameters for sample weight updates (outer loop). For the step learning rate scheduler (StepLR), we simply decay the learning rate by a factor of 10 every 30 steps.

Dataset	optimizer	lr	scheduler	grad clip	τ	steps
Waterbirds	GD	1	StepLR	1	0.1	100
CelebA	GD	1	StepLR	1e-2	0.01	100
MultiNLI	GD	0.1	StepLR	1e-2	1	50
CivilComments	GD	1	StepLR	1e-1	0.1	50

Table 4: Hyperparameters for last-layer retraining (inner loop)

Dataset	optimizer	lr	scheduler	batch size	weight decay	line search
Waterbirds	L-BFGS	1e-4	Constant	full	1e-1	Strong Wolfe
CelebA	L-BFGS	1e-4	Constant	full	1e-2	Strong Wolfe
MultiNLI	L-BFGS	1e-4	Constant	full	1e-2	Strong Wolfe
CivilComments	L-BFGS	1e-1	Constant	full	1e-3	Strong Wolfe

B.3 Implementation details

Let d denote the dimension of θ. Let the size of the held-out training set be n here. To efficiently compute the influence scores for last-layer retraining, we adopt the following strategy:

1. Calculate the Hessian inverse $H^{-1}_{\hat{\theta}^*,w}$ of the weighted objective w.r.t $\theta = \hat{\theta}^*$. The Hessian has a dimension of $d \times d$.
2. Calculate the *per-sample* gradient of the *unweighted* objective w.r.t. $\theta = \hat{\theta}^*$ for the *training* set. This results in a $n \times d$ matrix.
3. Calculate the *per-group* gradient of the *unweighted* objective w.r.t. $\theta = \hat{\theta}^*$ for the *target* set. This results in a $m \times d$ matrix, where m is the number of groups.

By combining these three matrices, we obtain the group-wise influence scores as a $n \times m$ matrix, which can then be aggregated as in Algorithm 1 and become an $n \times 1$ gradient vector.

B.4 RUNNING TIME COMPARISON

Hardware. For all experiments, we run on machines with NVIDIA RTX 3080 (10GB) / RTX A5000 (24GB) GPU and AMD EPYC 7543 CPU.

Running time. We record the detailed running time for both the inner and the outer loop for different datasets in Table 5. The results are obtained from running a single job on one NVIDIA RTX 3080 GPU with two AMD EPYC 7543 CPUs.

Table 5: Running time for `GSR`

Dataset	Dataset stats			Running time (s)		
	Held-out size	Target size	# of steps	Outer loop	Inner loop	Total
Waterbirds	479	600	100	2.71	0.16	285
CelebA	16277	9934	100	4.03	0.52	451
MultiNLI	20617	46231	50	7.24	0.53	381
CivilComments	26903	22590	50	8.21	0.7	882

Scalability. As we used `Pytorch` for our implementation and the last-layer retraining has very few parameters, the per-sample gradient and the Hessian inverse calculation involves high CPU usage, even though the tensors are on GPU. When the same processes are running in parallel, the performance sometimes can be CPU-bound instead of GPU-bound. Thus, the running time is likely to increase when the CPU-usage is high.

B.5 DETAILED RESULTS

In addition to the worst-group accuracy shown in the main paper, we also report the mean accuracy for these datasets in Table 6 for reference. We would like to highlight that the worst-group accuracy gain is usually at the expense of the average accuracy, which usually corresponds to no distribution shifts. This implies that trade-offs generally need to be made for better robustness to subpopulation shifts.

C UNDERSTANDING THE ROLE OF THE INVERSE HESSIAN

Koh & Liang (2017) analyzed that the inverse Hessian measures the robustness of the resultant model to upweighting the training data. As Hessian is a symmetric matrix, according to the Spectral Theorem, it guarantees the existence of an orthonormal basis of the eigenvectors. Hence, the gradient can be written as a linear combination of eigenvectors. As the influence function utilizes the inverse Hessian, which has the reciprocal of the eigenvalues of the Hessian, the influence score has a *larger* magnitude when the gradient of the training and test points are similar and along the direction of the eigenvectors with *smaller* magnitudes.

Having smaller eigenvalues can be interpreted as the first-order gradient changing relatively slowly. From the optimization perspective (Newton's method), this usually means we are allowed to take larger gradient steps when the trajectory has less variation with a smoother curvature. On the other hand, the step size is smaller when the curvature changes more quickly, indicating a more complex loss landscape.

If the Hessian is dropped in between the inner product of the gradient as in Equation 2, then we fail to account for the variations of step sizes in different directions specified by the eigenvectors. Thus, the outer loop gradient becomes incorrect and the optimization will be less reliable.

D VISUALIZATION OF THE SPURIOUS CORRELATIONS

We show an illustration of the spurious correlations for the Waterbirds dataset in Figure 5.

Table 6: **Performance comparison in detail.** We report the worst-group accuracy on four benchmark datasets. For the group label column, ✗ indicates no group label g is used; ✓ indicates g is required for training or validation; ✓̸ indicates g is partially used; ✓✓ indicates a proportion of g from the validation set is re-purposed beyond hyperparameter tuning, such as training sample weights or model parameters. The row sections are ranked in descending order of the total amount of group label information required.

Method	Group Label	Waterbirds		CelebA		MultiNLI		CivilComments	
	Train / Val	Worst(%)	Mean(%)	Worst(%)	Mean(%)	Worst(%)	Mean(%)	Worst(%)	Mean(%)
RWG	✓/ ✓	$87.6_{\pm 1.6}$	–	$84.3_{\pm 1.8}$	–	$69.6_{\pm 1.0}$	–	$72.0_{\pm 1.9}$	–
Group DRO	✓/ ✓	$91.4_{\pm 1.1}$	$93.5_{\pm 0.3}$	$88.9_{\pm 2.3}$	$92.9_{\pm 0.2}$	$77.7_{\pm 1.4}$	$81.4_{\pm 0.1}$	$70.0_{\pm 2.0}$	$89.9_{\pm 0.5}$
JTT	✗/ ✓	86.7	93.3	81.1	88.0	72.6	78.6	69.3	91.1
CnC	✗/ ✓	$88.5_{\pm 0.3}$	$90.9_{\pm 0.1}$	$88.8_{\pm 0.9}$	$89.9_{\pm 0.5}$	–	–	$68.9_{\pm 2.1}$	$81.7_{\pm 0.5}$
SSA	✗/ ✓✓	$89.0_{\pm 0.6}$	$92.2_{\pm 0.9}$	$\mathbf{89.8}_{\pm 1.3}$	$92.8_{\pm 0.1}$	$76.6_{\pm 0.7}$	$79.9_{\pm 0.9}$	$69.9_{\pm 2.0}$	$88.2_{\pm 2.0}$
MAPLE	✗/ ✓✓	91.7	92.9	88.0	89.0	72.7	77.2	64.1	89.7
DFR	✗/ ✓✓	$\mathbf{92.9}_{\pm 0.2}$	$94.2_{\pm 0.4}$	$88.3_{\pm 1.1}$	$91.3_{\pm 0.3}$	$74.7_{\pm 0.7}$	$82.1_{\pm 0.2}$	$70.1_{\pm 0.8}$	$87.2_{\pm 0.3}$
GSR-HF	✗/ ✓✓	$87.5_{\pm 0.1}$	$97.7_{\pm 0.0}$	$86.3_{\pm 0.4}$	$91.5_{\pm 0.0}$	$74.7_{\pm 0.0}$	$80.6_{\pm 0.0}$	$68.9_{\pm 0.2}$	$89.1_{\pm 0.0}$
GSR	✗/ ✓✓	$\mathbf{92.9}_{\pm 0.0}$	$94.9_{\pm 0.1}$	$87.0_{\pm 0.4}$	$90.9_{\pm 0.0}$	$\mathbf{78.5}_{\pm 0.3}$	$79.8_{\pm 0.0}$	$\mathbf{71.7}_{\pm 0.6}$	$85.9_{\pm 0.4}$
ERM	✗/ ✗	$74.9_{\pm 2.4}$	$98.1_{\pm 0.1}$	$46.9_{\pm 2.8}$	$95.3_{\pm 0.0}$	$65.9_{\pm 0.3}$	$82.8_{\pm 0.1}$	$55.6_{\pm 0.6}$	$92.1_{\pm 0.1}$
ES SELF	✗/ ✗	$\mathbf{93.0}_{\pm 0.3}$	$94.0_{\pm 1.7}$	$83.9_{\pm 0.9}$	$91.7_{\pm 0.4}$	$70.7_{\pm 2.5}$	$81.2_{\pm 0.7}$	–	–

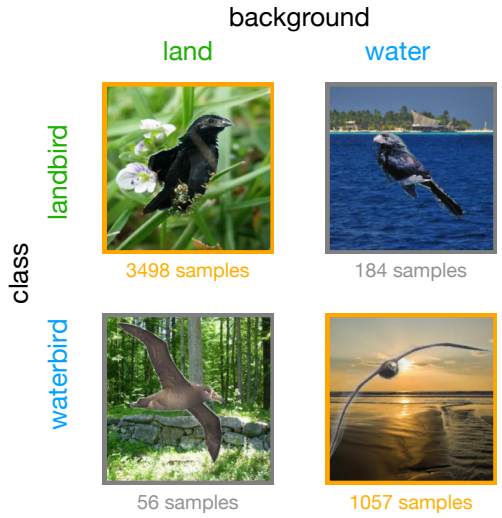

Figure 5: An illustration of the Waterbirds dataset. A spurious correlation exists between the bird class and the background. The majority groups are highlighted in orange. The minority groups are in gray.

E WHAT IF WE CAN RETRAIN THE FULL NETWORK WITH GSR?

In this section, we use a simple setup to explore the potential of retraining the full network with GSR, when the compute budget allows.

Setup. We conduct an ablation study on a small binary classification task customized from the ColoredMNIST, where the digits are spuriously correlated with color. We use a tiny Convolutional Neural Network (CNN) with 3 layers and about 5000 parameters.

Dataset. *ColoredMNIST-S*. We modify the original ColoredMNIST dataset (Arjovsky et al., 2019) by first taking only the first 6 digits out of all 10 digits, then assigning $y < 3$ as 0 and $y \geq 3$ as 1. The training, validation, and test splits have 10000, 2000, and 27375 instances, respectively. The spurious correlation γ is created by associating most of the instances in class 0 with red color and class 1 with green color. We set $\gamma = 0.1$ for the training split and set $\gamma = 0.5$ for the validation and test splits. we do not introduce any label corruption. This setting is considered much simpler than the original

Table 7: Performance comparison on ColoredMNIST-S Dataset with TinyCNN.

Method	ColoredMNIST-S	
	Worst(%)	Mean(%)
GSR-F-EH	**94.1**	96.0
GSR-F-AH	80.2	97.6
GSR-F-HF	91.9	96.9
GSR	91.2	95.4
GSR-HF	91.1	96.2
ERM	81.2	97.7

ColoredMNIST, primarily because we are studying with limited network capacity with a tiny CNN, which could not fit the original 10-digit classification with more than 90% accuracy.

Baselines. We compare GSR, which is by default trained with last-layer retraining, with the full-parameter retraining variants. GSR-F-EH retrains the entire network with the influence function and no approximation on the Hessian. We use Conjugate Gradients to calculate the inverse Hessian-vector product (iHVP) instead of explicitly calculating the Hessian to save compute the memory. GSR-F-AH approximates the Hessian using LiSSA (Agarwal et al., 2017) with depth=1000 and repeat=1. This approximation calculates the iHVP with 1000 samples from the training set. GSR-F-HF which discards the Hessian, and this uses the sample gradients as MAPLE.

The results are shown in Table 7. we can observe that. Full-parameter retraining with Hessian (i.e., GSR-F-EH) is advantageous over all other approaches. However, approximating the Hessian with low quality might hurt the performance, since GSR-F-AH underperforms other baselines. When using a small neural network model, last-layer retraining (LLR) can cause slight performance degradation when we have the capability to retrain the whole model on the entire dataset, but it is still significantly better than ERM.

F Comparison with MAPLE

Although the difference seems to be only about the Hessian, GSR and MAPLE are based on two distinct ways to solve the bilevel optimization problem.

1. MAPLE directly approximates backpropagating through the training trajectory by one-step truncation, but GSR uses implicit differentiation that results in the Hessian. This calculation is *exact* when the objective is strongly convex.
2. GSR also synergies with last-layer retraining, which was not considered by MAPLE.
3. We use an adaptive aggregation of the influence scores from the groups as the gradient, but MAPLE does not explicitly design group-level aggregation for subpopulation shifts.
4. MAPLE additionally uses coreset selection by training on a subset of all the training data in each step to speed up the training, while GSR utilizes the full training data without approximation.

G Additional dataset for subpopulation shift

To further demonstrate the advantage of GSR, we include an additional experiment with the *MetaShift* (Liang & Zou, 2022) image classification dataset. We use the two-class version implemented by Yang et al. (2023), where the spurious correlation exists between the class and the background. In particular, cats are mostly indoors and dogs are mostly outdoors. We primarily compare with DFR, which uses the same amount of group labels and the same ERM feature extractor as ours. The ERM model is trained for 100 epochs without early stopping or hyperparameter tuning. GSR outperforms DFR convincingly in this case as shown in Table 8.

Table 8: Performance comparison on MetaShift.

Method	**MetaShift**	
	Worst(%)	Mean(%)
GSR	$78.2_{\pm 4.0}$	$87.9_{\pm 4.1}$
DFR	$71.4_{\pm 1.6}$	$89.7_{\pm 0.2}$
ERM	69.2	90.3